frontiers | Frontiers in Earth Science

TYPE Original Research
PUBLISHED 12 January 2023
DOI 10.3389/feart.2022.1071228

Check for updates

OPEN ACCESS

EDITED BY
Faming Huang,
Nanchang University, China

REVIEWED BY
Avishek Adhikary,
National Institute of Technology,
Durgapur, India
Barna Heidel,
Esslingen University of Applied Sciences,
Germany

*CORRESPONDENCE
Bing Bai,
bbai@bjtu.edu.cn

SPECIALTY SECTION
This article was submitted to
Geohazards and Georisks,
a section of the journal
Frontiers in Earth Science

RECEIVED 16 October 2022
ACCEPTED 07 December 2022
PUBLISHED 12 January 2023

CITATION
Bai B, Bai F, Sun C, Nie Q and Sun S
(2023), Adsorption mechanism of shell
powders on heavy metal ions Pb^{2+}/Cd^{2+}
and the purification efficiency for
contaminated soils.
Front. Earth Sci. 10:1071228.
doi: 10.3389/feart.2022.1071228

COPYRIGHT
© 2023 Bai, Bai, Sun, Nie and Sun. This is
an open-access article distributed
under the terms of the Creative
Commons Attribution License (CC BY).
The use, distribution or reproduction in
other forums is permitted, provided the
original author(s) and the copyright
owner(s) are credited and that the
original publication in this journal is
cited, in accordance with accepted
academic practice. No use, distribution
or reproduction is permitted which does
not comply with these terms.

Adsorption mechanism of shell powders on heavy metal ions Pb^{2+}/Cd^{2+} and the purification efficiency for contaminated soils

Bing Bai[1]*, Fan Bai[1], Chenmiao Sun[1], Qingke Nie[2] and Shuo Sun[1]

[1]Key Laboratory of Urban Underground Engineering of Ministry of Education, Beijing Jiaotong University, Beijing, China, [2]China Hebei Construction and Geotechnical Investigation Group Ltd., Shijiazhuang, China

The adsorption capacity of oyster shell powders (SPs) and the adsorption mechanism of heavy metal ions (HMs; i.e., cadmium ions Cd^{2+} and lead ions Pb^{2+}) on SPs are discussed by means of adsorption kinetics tests, adsorption-desorption tests, scanning electron microscopy and Fourier transform infrared spectroscopy. The influences of seepage velocity, heavy metal types, and SP addition amount/concentration on the adsorption effect of SPs in the treatment of HMs in laterite as well as quartz sand were analyzed. Studies have shown that i) the adsorption of HMs on SPs can be divided into three stages, i.e., the surface adsorption stage, the internal pore diffusion stage, and the equilibrium stage; ii) with the increase in seepage velocity, the effluent concentration of HMs will slightly increase, and the residual amounts at each section of the column generally decrease rapidly with the increase in migration distance; iii) the increase in the concentration of SP solution provides more adsorption points for the adsorption of HMs, and finally, the amount of HMs desorbed from quartz sand is reduced, which also reduces the concentration of HMs in the effluent. Overall, SPs possess high purification efficiency for the HMs of contaminated soils.

KEYWORDS

shell powder, heavy metal ion, adsorption mechanism, static adsorption, dynamic adsorption

Highlights

1 The dynamic adsorption process of HMs on SPs was assessed based on microstructures.
2 Competitive adsorption mechanisms between SPs and laterite were explored.
3 The toxic leaching harmfulness of the solidified HMs in an acidic environment was evaluated.
4 The purification process of contaminated soil by SPs under seepage flow was revealed.

1 Introduction

Heavy metal ions (HMs) in soils have a long residual period and strong toxicity and easily migrate, which makes heavy metal pollutants easily flow into the food chain and ultimately affect human life and health (Huang et al., 2020a; Huang et al., 2020b; Khirul et al., 2020; Wang et al., 2021; Deng et al., 2022). A large part of the land polluted by heavy metals is cultivated land and accounts for 8% of the total cultivated land in China (Liu, 2015; Yu et al., 2021; Bai et al., 2022a), resulting in the reduction of grain production and the decline of grain quality (Jiang et al., 2018; Huang et al., 2020c; Rodriguez-Arellao et al., 2021; Wang et al., 2022). According to the Bulletin of National Soil Pollution Survey, the total soil that exceeds the Chinese standard of soil pollution is as high as 16.1%. These polluted soils are mainly polluted by inorganic substances; 82.8% of the polluted soils exceed the standard for inorganic substances. Among inorganic pollutants, 7.0% of the soils exceed Cd^{2+} standards (less than 0.3 mg/kg) and 1.5% exceed the Pb^{2+} standards (less than 35 mg/kg). Solidification-stabilization is the most effective, extensive and low-cost method for the treatment of heavy metal pollution in soil (Meski et al., 2019).

At present, the most commonly used solidification materials are cement-based materials such as cement and lime (Chang et al., 2020; Hu et al., 2021a; Zhong et al., 2021; Xue et al., 2022). Although these materials have a good solidification effect, they also bring new pollution problems and consume a lot of energy and produce harmful gases such as soot and sulfur dioxide (Xu et al., 2019; Bai et al., 2021a; Hu et al., 2021b). Khan and Jones (2009) studied the method of solidifying copper, iron, zinc and lead ions in the soil by adding organic fertilizer, lime, diammonium phosphate and other solidifying agents to the soil samples of a copper mine. Their research found that lime has clear advantages in reducing levels of copper, iron and zinc, while diammonium phosphate has a clearer effect in reducing the effective lead ion levels as well as the presence of very fine particles in porous media (Cui et al., 2019; Cui et al., 2022a; Bai et al., 2022b). Abdelhafez et al. (2014) showed that bagasse and orange peel biochar can effectively improve the stability, water holding capacity and cation exchange capacity of soil, and bagasse biochar can also effectively reduce the solubility of Pb^{2+}, which can bring the concentration of Pb^{2+} below the toxic leaching level of the toxicity characteristic leaching process (TCLP). However, the addition of two kinds of biochar will lead to desorption of arsenate and enhance the mobility of arsenic ions, which should be given special attention.

Moon et al. (2013a) used oyster shell powder (SP) and cow bone to make a mixed solution to treat Pb^{2+} and Cu^{2+} in soil. The results showed that the leaching rates of Pb^{2+} and Cu^{2+} decreased by 99% and 96%, respectively, when a mixed solution of 5% oyster SP and 5% waste bovine bone powder was used for pollutant treatment (Moon et al., 2013b). Torres-Quiroz et al. (2021) treated heavy metal-contaminated soil with oyster SP, zeolite and red mud and evaluated its solidification effect by using the leaching method of toxic characteristics. The results showed that oyster SPs could solidify 82% Pb^{2+} and 78% Cu^{2+}, while zeolite had a good curing effect on Pb^{2+}. Hong et al. (2010) studied the adsorption effect of oyster SP and calcium hydroxide on Cd^{2+}, which showed that oyster SP is less capable of improving soil pH and net negative charge than calcium hydroxide but better than calcium hydroxide in reducing the extractability of Cd^{2+}. Lee et al. (2018) studied the adsorption effect and adsorption mechanism of oyster SP when adsorbing Cd^{2+}. By analyzing the X-ray diffraction pattern, they found that oyster SP will produce precipitation when adsorbing Cd^{2+}, and precipitation will occur when the adsorption reaction occurs, indicating that chemical adsorption is the main mechanism of Cd^{2+} solidification by oyster SP. Ahmad et al. (2013) studied the adsorption capacity of oyster SP and calcined oyster SP on antimony in soil, which showed that oyster SP increased the leaching capacity of antimony, while calcined oyster SP decreased the leaching capacity of antimony.

In general, the use of SP as a new adsorption material has also received much attention. However, there are still gaps in the research on the penetration adsorption effect of SPs in porous media and the time-varying effect of SPs on the solidification of heavy metals in soil (Bai et al., 2021b). The following are reported in this paper: i) three kinds of SPs (small particle size SP, calcined SP and natural SP) are preliminarily selected to determine the adsorption capacity and stability of heavy metal pollutants in the adsorption solution and the SPs with the best adsorption effect are determined; ii) for the selected SPs, the adsorption-desorption test and model fitting were carried out, and then the mechanism of adsorption of HMs on SPs was analyzed by scanning electron microscopy (SEM) and Fourier transform infrared (FTIR) spectroscopy; iii) the leaching test and toxicity characteristic leaching test were carried out on contaminated soil to determine the content of leachable HMs in the soil samples and the influence of time and SP amount on the stable solidification of HMs; and iv) through the soil column test, the cleaning process of HMs by SPs under the condition of seepage water flow and the residues of HMs and SPs at different cross sections were analyzed.

2 Materials and methods

2.1 Test materials

Laterite, as the material used in static adsorption tests, contains many clay minerals. Laterite has many micropores, a high specific surface area and a strong cation exchange capacity, and colloidal clay can effectively adsorb HMs in groundwater leachate. The laterite used in this test was purchased from Lingshou County, Hebei Province, China. The specific gravity of the soil is 2.71 (pycnometer test method), the plastic limit is

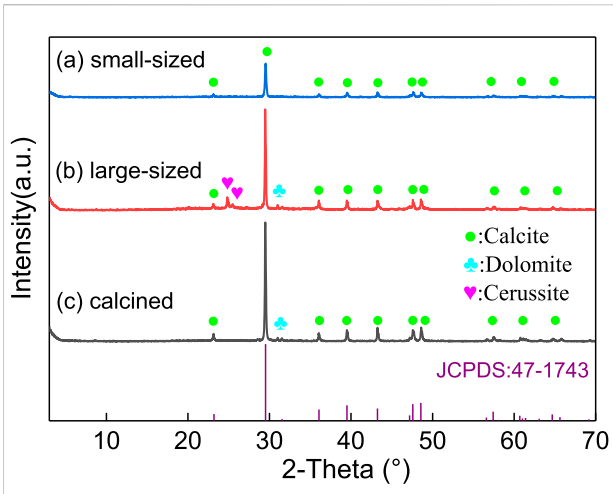

FIGURE 1
XRD patterns of **(A)** small, **(B)** large, and **(C)** calcined SPs.

21.5%, the liquid limit is 57.3% (photoelectric combined liquid-plastic limit tester), and the plastic index is 35.8. The oxide composition of the laterite measured by X-Ray Fluorescence (XRF) is Al_2O_3 (46.42%), SiO_2 (40.7%), Fe_2O_3 (10.89%), TiO_2 (0.77%), K_2O (0.67%), CaO (0.4%), MnO (0.09%), SrO (0.04%), and ZnO (0.02%).

Quartz sand is a non-metallic mineral formed by crushing natural quartz stone. Its main component is SiO_2 (accounting for more than 99.9%). Quartz sand is stable, hard, translucent and insoluble in water. Quartz sand is used as the matrix for the soil column penetration test in this study and has a particle size range of 0.5 –3 mm, a porosity of 41.54% and a solid particle density of 2.14 g/cm^3. The curvature coefficient C_c=1.16, average particle size D_{50}=1.79 mm and the non-uniformity coefficient C_u=1.81 less than 5, which show that the particle size distribution is relatively uniform.

Two kinds of HMs, Cd^{2+} and Pb^{2+}, which are common and serious soil pollutants, were selected for this study. The Cd^{2+} solution is prepared by adding cadmium nitrate ($Cd(NO_3)_2$) hydrate crystals into deionized water. The Pb^{2+} solution is prepared by adding lead acetate ($Pb(CH_3COO)_2$) hydrate crystals into deionized water.

China has a large output of shells. SPs have a high content of calcium carbonate, and there are a large number of pores in the powder particles. Therefore, SPs have certain advantages in the adsorption of heavy metal pollutants. The oyster SP used in the experiment was obtained from oyster shells in Dalian Bay, Liaoning Province, China, which were crushed and ground. The small SP is obtained by ball milling the oyster SP, and its maximum particle size is 6.5 μm. The particle size is very small, and solid particles are nearly invisible when dissolved in water. As a comparison, two other kinds of SPs (calcined SP and large natural SP) with a maximum particle size of 350 μm were selected for comparison (Li et al., 2017; Fan et al., 2021). Large natural SP was not subjected to grinding, and calcinated SP was subjected to calcination (700°C); the solid particles of these two SPs can be observed in water. According to X-ray diffraction (XRD), the mineral composition of the three SPs is mainly calcite (Figure 1). The small natural SP consists of calcite (76%), dolomite (6%), galena (3%) and microcline (15%); large natural SP consists of calcite (76%), dolomite (6%), galena (3%), and microcline (15%); and calcined SP consists of calcite (96%) and dolomite (4%).

2.2 Test apparatus

A magnetic agitator (Model CCJ78-1 produced by the Jintan Co., Ltd, China) was used for the static adsorption test, with a rotating speed of 0–2000°r/min and a controlled temperature range of 0–75°C (Bai X. et al., 2021; Bai et al., 2022a). The purpose is to improve the contact between the particles and the solution and form a stable adsorption state. A turbidimeter was used to measure the turbidity of the SPs in the solution and then convert the corresponding concentration. The turbidimeter is a Hach2100 produced by the American Hach Company, with a measurement range of 0–4000 NTU.

The VP-10 L vacuum suction filter pump produced by Qun'an Experimental Instrument Co., Ltd. and the supporting filter device are used for sample filtration. A TAS-990 graphite furnace atomic spectrophotometer produced by Beijing Puxie General Instruments Co., Ltd. is used to measure the concentrations of Cd^{2+} and Pb^{2+}, and its absolute sensitivity can reach 10^{-1}–10^{-5} ng.

Using FTIR spectroscopy, the functional group changes of SPs soaked in deionized water, standard Cd^{2+} solution and standard Pb^{2+} solution were analyzed. The scanning range was set at 500 –4000 cm^{-1}, and then the changes in the SPs during the adsorption of Cd^{2+} and Pb^{2+} were analyzed (Yakub et al., 2020; Bai et al., 2021a).

The SPs obtained in the experiment were centrifuged, and then the amount of HMs stripped from the disturbed SPs was measured. The L3-6 K low-speed centrifuge produced by Hunan Kecheng Instrument Equipment Co., Ltd. was used. The test speed was set at 4000 r/min, and the centrifugation time was set at 5 min. The supernatant after centrifugation was filtered, and then the concentration of HMs was determined by a TAS-990 graphite furnace atomic-absorption spectrophotometer (manufactured by the Persee General Instrument Co., Beijing, China) after dilution.

2.3 Adsorption kinetics test

Cd^{2+} and Pb^{2+} solutions with a concentration of 50 ng/ml were prepared, and the beaker containing the solution was magnetically stirred. The temperature was set at 25°C, and the

rotating speed was set at 200 r/min. Then, 0.5 g SP was added to the fully stirred HM solution. The stirring time was at least 30 s and continued until no agglomerated SPs were observed in the solution. Tests were performed three times, and the average value was taken as the final result (Dehghan et al., 2021; Wu et al., 2021).

After the SP was fully dispersed in the solution, samples were taken at predetermined time intervals. An approximately 5 ml sample was taken from the middle of the solution with a pipette gun and then filtered through a 0.45 μm microporous membrane for vacuum filtration to further remove the SPs. The concentration of HMs was then determined.

The SP residue after filtration was taken for the adsorption stability test. To this end, 100 mg was taken for drying and then put into a centrifuge tube, and deionized water was added to reach 30 ml. The mixture was placed on an oscillator (150 r/min) for 1 h and then centrifuged at 4000 r/min for 5 min. The HM concentration in the supernatant was then measured.

2.4 Dissolution test and toxic leaching test method

The dissolution test was used to detect the concentration of HMs after the soil sample was dissolved in deionized water. The toxic leaching test was used to detect the concentration of HMs after the soil sample was washed with a strong acid. Based on the difference between the concentrations of dissolved/leached from the two tests, the ability of soil as well as contaminated soil with SPs to solidify HMs can be analyzed (Bashir et al., 2018; Li et al., 2018; Mehmood et al., 2019).

According to the Chinese test standard "solid waste-extraction procedure for leaching toxicity sulfuric acid and nitric acid method" (State Environmental Protection Administration, 2007a; HJ/T299-2007), 25 g of sample particles was added into 250 ml of mixed sulfuric/nitric solution (i.e., toxic leaching test) for dissolution treatment or deionized water (dissolution test) for comparison. After shaking, 10 ml of solution was placed into a centrifuge tube for centrifugation at 4000 r/min for 5 min. Then, the supernatant was removed and poured into a vacuum suction filtration device for filtration. Thus, the concentration of HMs was determined. For the raw soil, the contents of Cd^{2+} and Pb^{2+} in the leaching solution were 0.009 and 0.0176 μg/ml, respectively, which were negligible relative to the contaminated soil sample prepared later.

Cd^{2+} or Pb^{2+} (cadmium nitrate tetrahydrate with a mass of 28 g and lead acetate trihydrate with a mass of 32 g) was dissolved in 3500 ml deionized water, and then the solution was added to laterite (mass of 16 kg) in 10 divisions step by step and completely stirred with a mixer (200 r/min) for 5 min. After mixing, the soil samples were dried, crushed and screened (with a 0.074 mm filter) to form contaminated soil samples. Then, the dissolution test and toxic leaching test were carried out. The results showed that the concentrations of HMs in the polluted laterite dissolved with deionized water were 0.622 μg/ml for Cd^{2+} and 0.461 μg/ml for Pb^{2+}. In fact, the pollution degree of Cd^{2+} in polluted soil is often higher than that of Pb^{2+} and therefore deserves more attention. After strong acid leaching, the concentrations of HMs were 20.9 and 11.9 μg/ml for Cd^{2+} and Pb^{2+}, respectively. The two concentrations were both greater than the limit given by the leaching toxicity criterion (State Environmental Protection Administration, 2007b; GB 5085.3–2007); thus, the samples can be considered hazardous waste.

To investigate the solidification effect of SP on HMs, six samples composed of small-sized SP and contaminated soil with different proportions were selected for the experiment: laterite contaminated by Cd^{2+} and Pb^{2+} (soil samples 1 and 2, respectively); laterite contaminated by Cd^{2+} and Pb^{2+} mixed with 5% SP (soil samples 3 and 4, respectively); and laterite contaminated by Cd^{2+} and Pb^{2+} mixed with 10% SPs (soil samples 5 and 6, respectively). The mixed samples were stirred thoroughly with a stirrer and then placed in the incubator layer by layer. For each layer, deionized water was sprayed evenly to keep the soil sample moist and ensure that the soil moisture content was kept at 20% when the final filling was completed.

Six groups of configured soil samples were subjected to static treatment at room temperature (25°C). The moisture content was measured every 5 days during this period. If necessary, an appropriate amount of deionized water was added to ensure that the moisture content was maintained at 20%. Samples were taken at 0, 1, 7, 14 and 28 days for detection. For this purpose, samples were taken from five measuring points, such as the four corners and the center of the soil sample, and their average values were taken as the final values. The obtained samples were divided into two parts: one part was dissolved in deionized water for the dissolution test, and the other was used for the toxic leaching test. Acid leaching can largely destroy the unstable structure of soil samples, maximizing the release of the adsorbed HMs, while the undecomposed HMs were considered to be in the stable solidified part.

2.5 Soil column test

The adsorption of HMs on SP in porous media was studied by a sand column penetration test. The sample has a diameter of 10 cm and a length of 90 cm. The quartz sand washed with deionized water was put into the oven for drying for 24 h (105°C) to avoid the possible influence of impurities on the results, and loaded into the sand column in layers, and each section of the sand column was loaded in 10 layers. After each layer of sand loading was completed, uniform compactness was ensured by using a compaction hammer.

Before the formal test, deionized water was injected into the sand column through the peristaltic pump at a seepage velocity of

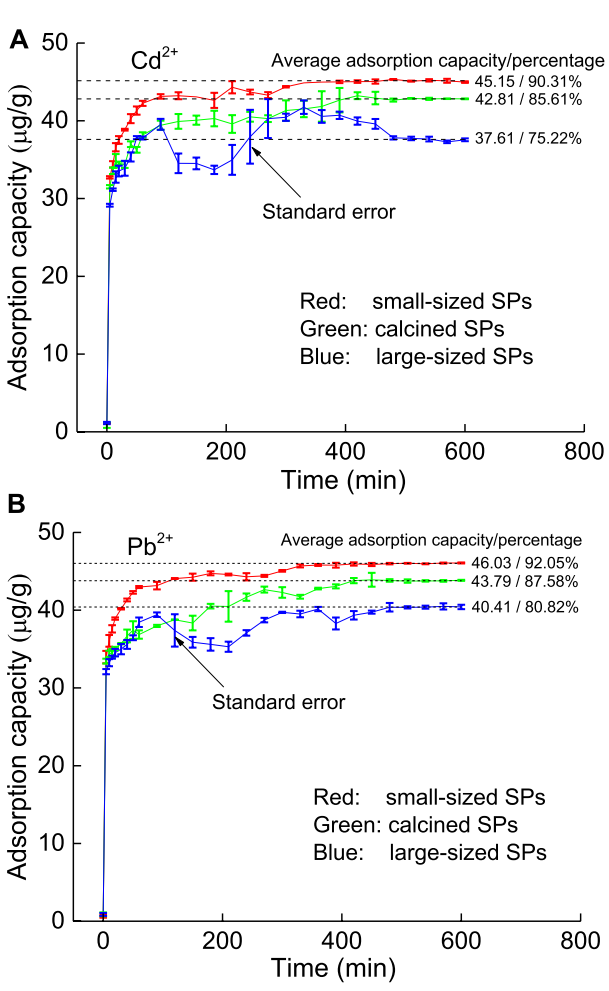

FIGURE 2
Adsorption capacity of small, large and calcined SPs for **(A)** Cd^{2+} and **(B)** Pb^{2+}.

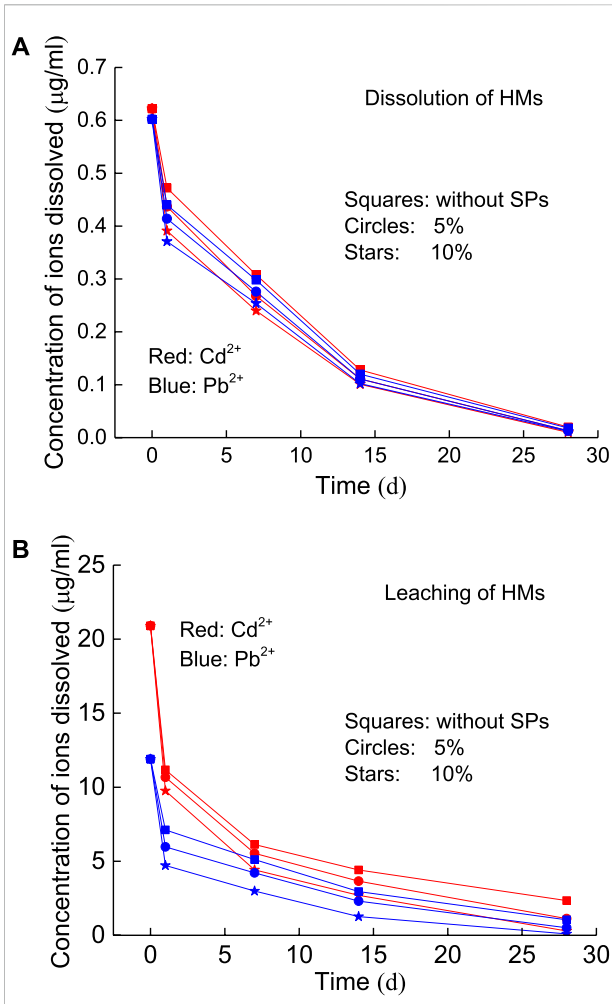

FIGURE 3
The dissolved amount of HMs with time: **(A)** dissolution of HMs and **(B)** leaching of HMs.

v=0.08 cm/s for full flushing. At the same time, the leachate was removed at the lower end of the sand column until the turbidity was less than six NTU, at which point it was considered that the column had been washed clean. HM (Cd^{2+} or Pb^{2+}) solutions were injected at a certain concentration (C=100, 200, or 400 ng/ml) and seepage velocity (v=0.04 or 0.08 cm/s) from the upper end of the sand column. At the same time, a sampling bottle with a capacity of 30 ml was used at the lower end of the sand column to obtain the effluent at a predetermined time interval (e.g., 30 s). The turbidity of the effluent was measured with a turbidimeter and then filtered with a vacuum suction filter. The content of HMs in the filter solution was determined by a graphite furnace atomic spectrophotometer. After the test, the contaminated sand column was disassembled, quartz sand samples were taken 0, 30, 60 and 90 cm away from the injection surface, and then the residual concentration of HMs was measured.

The peristaltic pump used was a BT600-2 J type produced by Baoding Lange Constant Flow Pump Co., Ltd. The selected seepage velocities were 0.040 cm/s and 0.080 cm/s. The soil column was washed with SP solution at the concentrations of C_{SP}=0, 0.5, 1.0, and 1.5 mg/ml for each seepage velocity. After the completion of the test, the concentration of HMs at each section was also measured, and the residual concentration of SPs was obtained simultaneously.

3 Static adsorption, dissolution and leaching of HMs by SPs

3.1 Static adsorption

The adsorption amount of HMs is defined as

$$q = (C_0 - C) \cdot \frac{V}{m} \quad (1)$$

where q (μg/g) is the amount of HMs adsorbed per unit mass of SP at adsorption time t (min), C_0 is the initial solution concentration (ng/mL), C is the solution concentration during adsorption (ng/mL), V is the solution volume (mL), and m is the mass of the SP (g).

$C = C_e$ denotes the equilibrium concentration of HMs in the solution (ng/mL). Figure 2 gives the adsorption capacity of the three selected SPs with time and the standard errors of three parallel tests. For large SPs, the adsorption efficiency of Cd^{2+} and Pb^{2+} is the highest in the first stage (e.g., 5 min). Then, the growth of adsorption capacity gradually slowed down and then rapidly declined after reaching a peak. After the decline, there was another plateau that returned to a high level again and slowly reached a stable state. Finally, the adsorption rates reached steady values of 37.61 μg/g and 40.41 μg/g (i.e., 75.22% and 80.82%) for Cd^{2+} and Pb^{2+}, respectively. The adsorption process of HMs on the large SPs has a large fluctuation due to the limited number of adsorption sites that large-sized SP can provide, coupled with the high energy required for intraparticle diffusion, the smoothness of the curve in the adsorption process is very poor, and the time to reach stability is also long (e.g., 800 min). In addition, the adsorption trend of Pb^{2+} on SPs is similar to that of Cd^{2+}, but the fluctuation range is also smaller.

Similar to the large natural SP, for calcined SP and small natural SP, there is a high-efficiency adsorption stage in the first stage, and then the adsorption capacity increases slowly with increasing time with a small fluctuation range. Overall, the adsorption capacity of the small natural SP is better than that of calcined SP. Hence, small natural SP is used as the final purification material.

3.2 Dissolution of HMs

As shown in Figure 3A, with increasing time, the concentration of HMs dissolved from the laterite sample decreases, which indicates that the addition of SP makes it more difficult for HMs to convert to a free state. In the three cases (no SP, adding 5% SP, adding 10% SP), the adsorption processes of Cd^{2+} and Pb^{2+} were slightly different, which confirmed that the adsorption mechanism for the two HMs on SP was also different. The concentration of HMs tends to be the same at 28 days, indicating that with increasing time, the inhibition of SP weakens the transformation of HMs to the free state. At 28 days, the amount of HMs dissolved in deionized water was 0.02 μg/ml, which was 3% of the initial concentration.

As a comparison, the laterite sample in the dry state (when the moisture content is zero) is also tested with the addition of 5% SP and 10% SP. The test results showed that the concentration of the dissolved HMs after standing for a long time (e.g., 28 days) was almost the same as that of the initial configuration sample. This displayed that there is no adsorption reaction between laterite, SP and HMs in the dry state, indicating that the water content is also a necessary condition for the adsorption reaction.

3.3 Leaching of HMs

The amount of dissolved HMs from the laterite sample after acid leaching treatment decreases with time (Figure 3B). After 28 days of standing, the concentrations of Cd^{2+} in the three cases (no SP, 5% SP and 10% SP) after acid leaching treatment were 2.34, 1.13 and 0.29 μg/ml, respectively. This decrease in Cd^{2+} concentration with increasing SP content is because more HMs can be stably solidified by chemical adsorption and intraparticle diffusion, so the concentration of HMs in the leaching solution will be reduced. After that, with the decrease in adsorption sites and the long time required for particle diffusion, the subsequent adsorption rate gradually decreased.

The micropores of laterite grant it a high adsorption capacity, so the concentration of HMs leached is also reduced at 28 days. The ability to solidify HMs can be further improved by adding SP. As shown in Figure 3B, the leachable amount of HMs from the laterite samples after 1 day of standing decreased significantly, and then the declining rate gradually slowed down. In the case of no SP, the leaching concentration of Cd^{2+} is still higher than the concentration limit of hazardous substances (i.e., 1 μg/ml) (State Environmental Protection Administration, 2007b; GB 5085.3–2007), while the leaching concentration of Pb^{2+} after standing for 14 days is 2.95 μg/ml, lower than the concentration limit of hazardous substances (5 μg/ml). After adding 10% SP, the Cd^{2+} leaching concentration was 0.29 μg/ml after standing for 28 days, lower than the concentration limit of hazardous substances (State Environmental Protection Administration, 2007b; GB 5085.3–2007).

Compared with the dissolution test (Figure 3A), the concentration of HMs obtained by the toxicity leaching test is much higher (Figure 3B); that is, there will be more HMs in the acid soil. Hence, the harm of HMs in the low pH environment will be amplified.

3.4 Adsorption mechanism of HMs onto SPs

The adsorption process of HMs onto SPs can be fitted by a quasi-first-order adsorption kinetic model, quasi-second-order adsorption kinetic model and Weber-Morris intraparticle diffusion model (Sarkaya, 2021; Zhou et al., 2021; Cui et al., 2022b), written as follows:

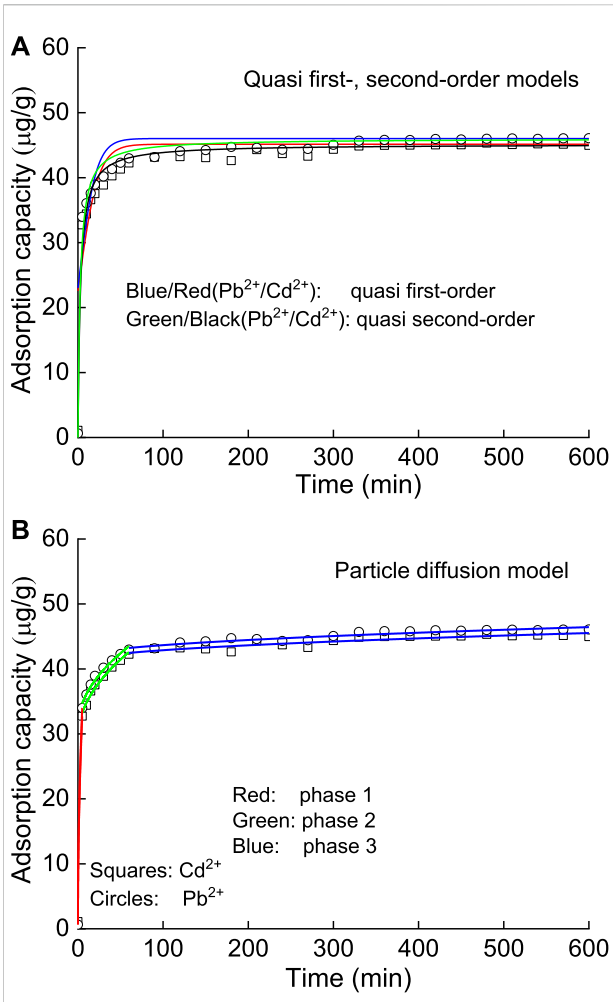

FIGURE 4
Particle diffusion model piecewise fitting diagram for different kinetic models: **(A)** quasi first- and second-order and **(B)** particle diffusion.

$$\log(q - q_e) = \log q_e - K_1 \cdot t \tag{2}$$

$$\frac{t}{q_e} = \frac{1}{K_2 \cdot q^2} + \frac{t}{q} \tag{3}$$

$$q_e = K \cdot t^{1/2} + C \tag{4}$$

where q_e is the amount of HMs adsorbed per unit mass of SP when the adsorption reaches the equilibrium state (μg/g); K_1 is the quasi-first-order adsorption rate constant (min^{-1}); K_2 is the quasi-second-order adsorption rate constant ($g{\cdot}\mu g^{-1}{\cdot}min^{-1}$); K is the intraparticle diffusion rate constant ($\mu g/gmin^{1/2}$); and C is a parameter (μg/g).

The quasi-first-order adsorption kinetic model describes the moving/attaching process of ions from the solution to the adsorbent surface, which is characterized as physical adsorption. The quasi-second-order adsorption kinetic model assumes that the adsorption rate is determined by the square value of the unoccupied adsorption vacancy on the adsorbent surface, which is controlled by chemical mechanisms such as electron sharing or electron transfer. The fitting results showed that the quasi-second-order adsorption kinetic model is better than the quasi-first-order adsorption kinetic model (Figure 4 and Table 1), which concluded that there is both physical and chemical adsorption during the process of HM adsorption on SP. It should be noted that the x-axis of the Weber-Morris model is obtained after squaring to ensure that the horizontal coordinates of the two plots are the same and to facilitate comparison.

Based on the significance of the particle diffusion model, the curves in the first stage cross the origin, and the adsorption is controlled by surface adsorption, which belongs to a physical process. The second is the internal pore diffusion stage, in which physical adsorption and chemical adsorption are combined, and at this time, the chemical adsorption of Cd^{2+} is more obvious than that of Pb^{2+}. The third stage is the equilibrium stage, in which the adsorption amount does not change significantly, and the adsorption is in dynamic equilibrium. The fitting curves of the second and third stages are not through the origin, so the adsorption is controlled not only by particle diffusion but also by chemical adsorption.

The higher the intraparticle diffusion rate constant K (Table 1) is, the faster the adsorption rate at this stage. This showed that the surface adsorption capacity of SPs to Pb^{2+} in the

TABLE 1 Adsorption kinetic model and the fitting parameters.

HMs	Kinetic model	K_1 (min-1)	K_2 (g·μg-1 min-1)	K (mg/g·min$^{1/2}$)			R^2
				Stage 1	Stage 2	Stage 3	
Cd^{2+}	quasi first-order	0.09621	-	14.14222	1.70589	0.18244	0.701
	quasi second-order	-	0.00813				0.980
	particle diffusion						
Pb^{2+}	quasi first-order	0.08557	-				0.712
	quasi second-order	-	0.00759				0.977
	particle diffusion			14.90564	1.60342	0.19144	

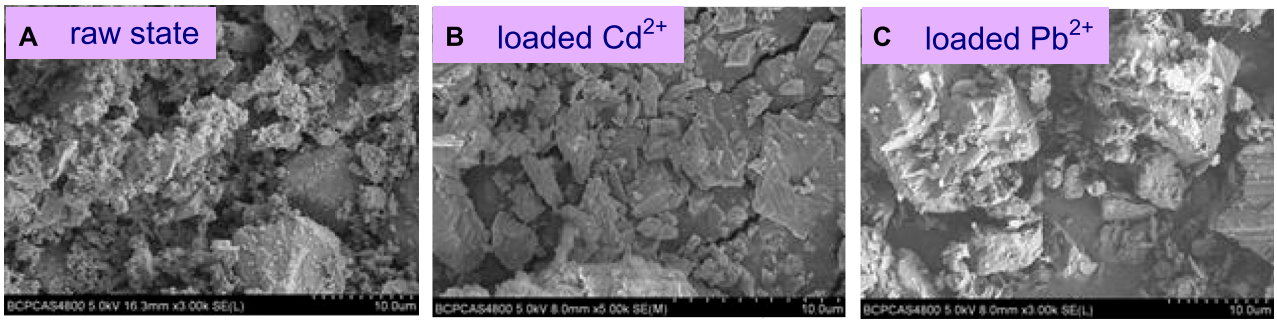

FIGURE 5
SEM images of SPs: **(A)** raw state, **(B)** loaded Cd^{2+}, and **(C)** loaded Pb^{2+}.

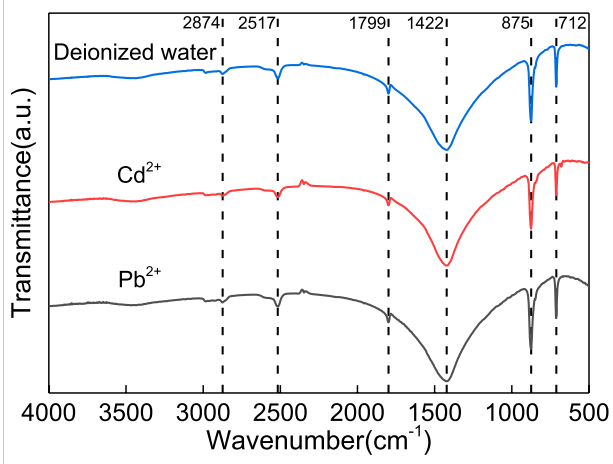

FIGURE 6
Fourier transform infrared spectroscopy of SPs soaked with deionized water, Cd^{2+} and Pb^{2+} solution.

first stage is better than that to Cd^{2+}, and the chemical adsorption of Cd^{2+} on SPs in the second stage is stronger than that of Pb^{2+}.

Figure 5 shows the SEM of SPs soaked in deionized water (i.e., raw state) and two HM solutions. There are many flocculent structures in the SPs soaked in deionized water. These flocculent structures are attached to the surface of the sheet structure. It is the existence of these flocculent structures that make the SPs have a large number of holes, which produce a large specific surface area and provide a large number of adsorption sites for the adsorption of HMs. As shown in Figures 5B,C, after loading with HMs (Cd^{2+} and Pb^{2+}), those flocculent structures disappear, and only flaky structures can be observed. This phenomenon occurs because these flocculent structures are stacked by small particles, which are not stable (Bai et al., 2022b). After they adsorb HMs, the original support is destroyed and laid on the surface of the sheet structure. In addition, due to the existence of chemical adsorption, ion exchange occurs between the SPs and solution, resulting in the production of new chemicals, which makes small particles with original flocculent structures accumulate on the surface of the sheet structure.

Comparing Figure 5C with Figure 5B, the flake structure of the SPs adsorbed with Pb^{2+} is very similar to that of the initial SPs (Figure 5A), while the flake structure of the SPs adsorbed with Cd^{2+} is more dispersed. This indicates that some lamellar structures of the SPs are broken after adsorption of Cd^{2+}. That is, due to the ion exchange reaction between Cd^{2+} and the original calcium carbonate of SPs, the original large flake structure is destroyed. This is consistent with the previous experimental results that the adsorption efficiency of Cd^{2+} is higher than that of Pb^{2+} (Figure 4) in the second stage of adsorption, which is mainly controlled by the chemical mechanism.

From the FTIR spectroscopy data shown in Figure 6, the characteristic peaks of SPs soaked in Cd^{2+} and Pb^{2+} are similar to those soaked in deionized water. This indicated that there is no significant change in the types of functional groups before and after adsorption, but there is a certain difference in their transmittance. For example, the transmittance of the original SPs at the characteristic peaks of 712, 875, 1422, 1799, 2517 and 2874 cm^{-1} are 63.97%, 34.85%, 10%, 58.08%, 71.26% and 74.90%, respectively, while the transmittance of the SPs soaked in Cd^{2+} solution is 70.97%, 41.43%, 10.03%, 61.45%, 68.62% and 69.74%, respectively. That is, some of the original chemical bonds in the SPs were destroyed, and an irreversible chemical reaction occurred between HMs and SPs, which once again confirmed that there was a strong chemical adsorption reaction between them.

In fact, both 712 cm^{-1} and 875 cm^{-1} are the characteristic absorption peaks of calcium carbonate. The former corresponds to the in-plane deformation vibration of O-C-O, and the latter corresponds to the out-of-plane deformation vibration of CO_3. The peak at 1422 cm^{-1} means that C-O is an antisymmetric stretching vibration peak. In fact, the C-O antisymmetric stretching vibration peak usually appears at 1458 cm^{-1}; that is, it produces a displacement of 36 cm^{-1} on the benchmark of 1422 cm^{-1}, and the absorption peak becomes wider, which is

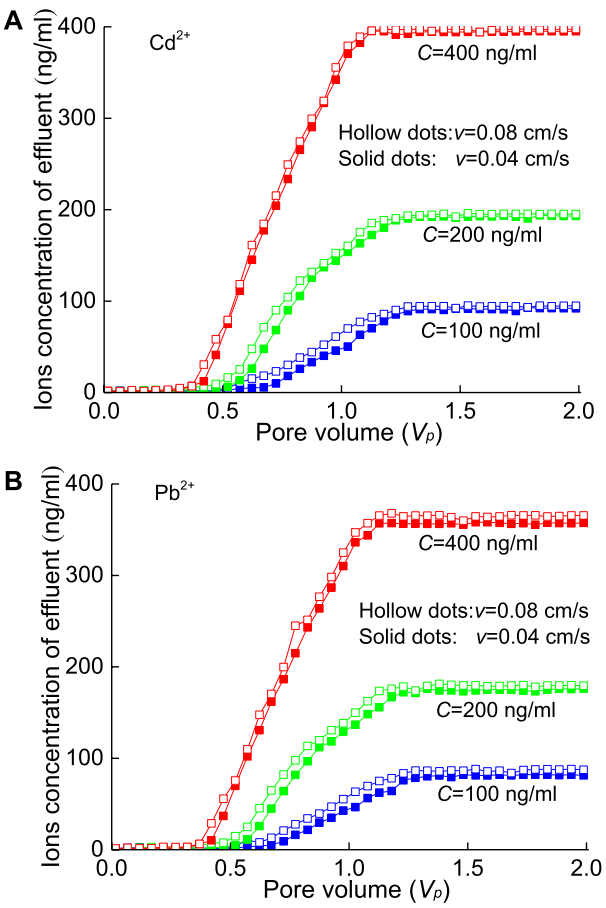

FIGURE 7
Effluent concentration during sand column pollution of HMs at different injection concentrations: **(A)** Cd^{2+} and **(B)** Pb^{2+}.

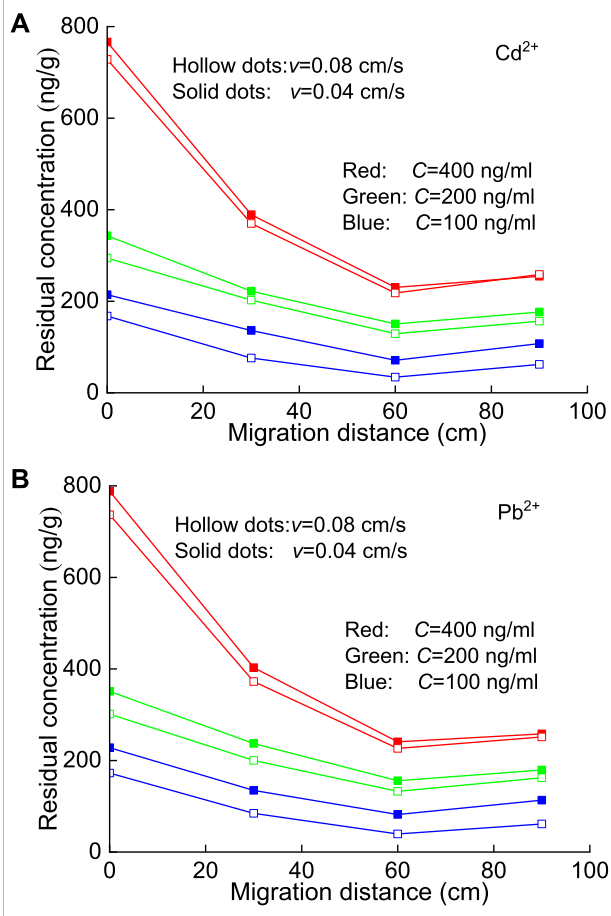

FIGURE 8
Residual concentration of HMs in each section of the sand column after pollution: **(A)** Cd^{2+} and **(B)** Pb^{2+}.

caused by lattice distortion of calcium carbonate crystals. The peak at 1799 cm^{-1} represents the C=O vibration peak in calcium carbonate, and the peaks at 2517 cm^{-1} and 2874 cm^{-1} do not belong to the characteristic absorption peak of calcium carbonate but instead correspond to the O-H vibration and $-CH_3$ symmetric stretching vibration peaks, respectively. Overall, the above characteristic peaks shows that the SPs are rich in calcium carbonate (de Oliveira et al., 2021; Li et al., 2021; Zhai et al., 2021; Zhang et al., 2021).

4 Adsorption of HMs by SPs under seepage flow

4.1 Effluent concentration of HMs in the soil column test

Through the long sand column penetration test, the adsorption effect of SP on HM pollutants in large-particle porous media was explored. Figure 7 shows the time-varying curves of the outflow concentrations during the injection of HMs (Cd^{2+} and Pb^{2+}) under seepage flow (v=0.04 cm/s and 0.08 cm/s). The abscissa is the pore volume (V_P), indicating the ratio of the total water flowing through the long sand column to the volume of quartz sand pores. Figure 7 indicates that the breakthrough curves of Cd^{2+} and Pb^{2+} solutions are similar; that is, is the curves have a rapid increasing stage and then tend to a steady state. Overall, the outflow concentrations of Cd^{2+} are slightly greater than those of Pb^{2+}, which indicates that the attachment of Pb^{2+} to quartz sand is stronger than that of Cd^{2+}. With the increase in seepage velocity (v=0.04→0.08 cm/s), the effluent concentration of HMs will increase slightly (Figure 7). This effect tends to be consistent with the increase in the injected HM concentration (e.g., C=400 ng/ml; i.e., the red curves in Figure 7).

Figure 8 shows that the residual amounts of Cd^{2+} and Pb^{2+} at each section of the column were very similar after the completion of the seepage test and generally decreased rapidly with increasing migration distance (e.g., 0→30→60 cm). Then, the

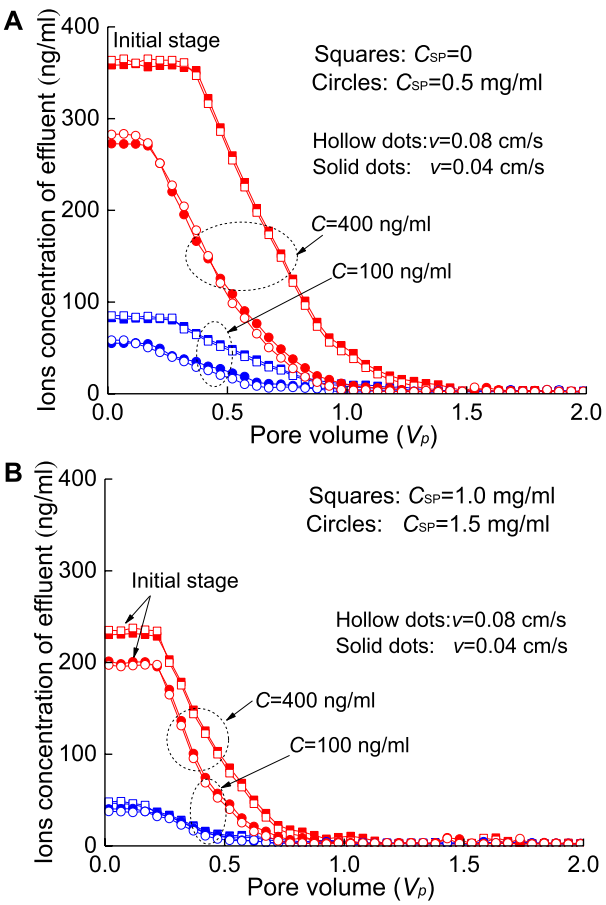

FIGURE 9
Effluent concentration of Cd^{2+}-contaminated sand column washed by SPs at different seepage velocities: **(A)** C_{SP}=0 and 0.5 mg/ml and **(B)** C_{SP}=1.0 and 1.5 mg/ml.

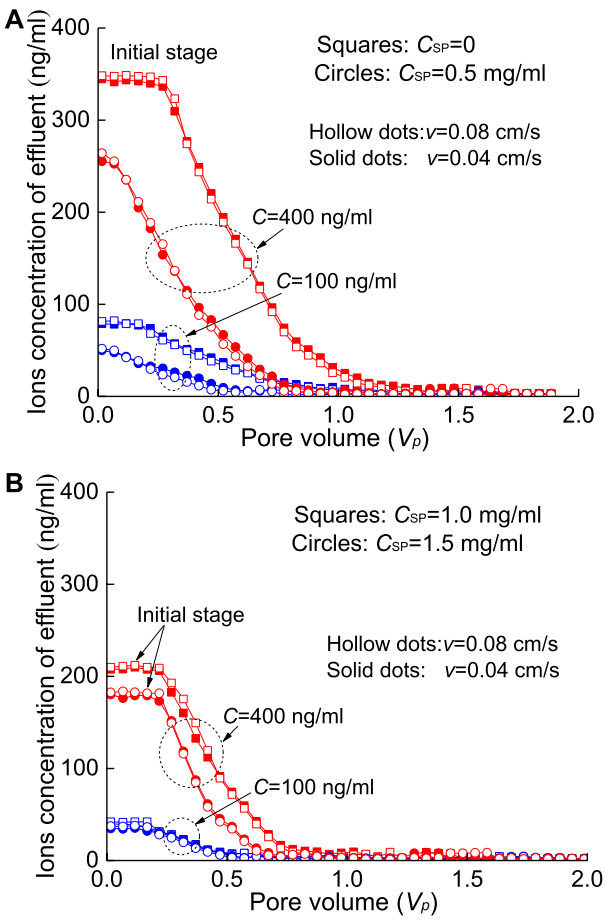

FIGURE 10
Effluent concentration of Pb^{2+}-contaminated sand column washed by SPs at different seepage velocities: **(A)** C_{SP}=0 and 0.5 mg/ml and **(B)** C_{SP}=1.0 and 1.5 mg/ml.

residual concentration at a greater distance (e.g., 90 cm) is slightly greater than that at the previous distance (e.g., 60 cm), which can be attributed to the accumulation of HM solution due to the existence of a filter screen. Certainly, the residual concentration of Pb^{2+} is slightly greater than that of Cd^{2+}.

4.2 Cleaning process of contaminated sand column

During the washing processes of the contaminated sand column with SP, the seepage velocity has little effect on the outflow concentration of HMs. The outflow concentrations of HMs under the two seepage velocities (i.e., v=0.04 cm/s and 0.08 cm/s) are similar in the initial stage (Figure 9 and Figure10) and denote a relatively steady process. The initial concentration of Pb^{2+} in the effluent is slightly lower than that of Cd^{2+}, where the increase in the concentration of SPs shows a strong adsorption for Pb^{2+}. In fact, the time in the washing process is relatively short, and the time in the dynamic adsorption process (i.e., seepage process) is far from the time required for the second stage adsorption in the particle diffusion model (Eq. 3); that is, only surface adsorption (i.e., physical interaction) occurs between SPs and HMs. Of course, under the present conditions, the SPs injected into the sand column mostly remain in the sand column.

The increase in the SP concentration provides more adsorption points for the adsorption of HMs. At the same time, more SP will be attached to the surface of quartz sand. Finally, the amount of HMs desorbed from quartz sand is reduced, which also reduces the concentration of HMs in the effluent. The penetration processes of the four SP solutions (C_{SP}=0, 0.5, 1, 1.5 mg/ml) are plotted in Figure 9 and Figure 10. Compared with the flushing results with deionized water (i.e., C_{SP}=0), the effluent concentration after adding SP (e.g., 0.5 mg/ml–1.5 mg/ml) clearly decreased in the initial stage

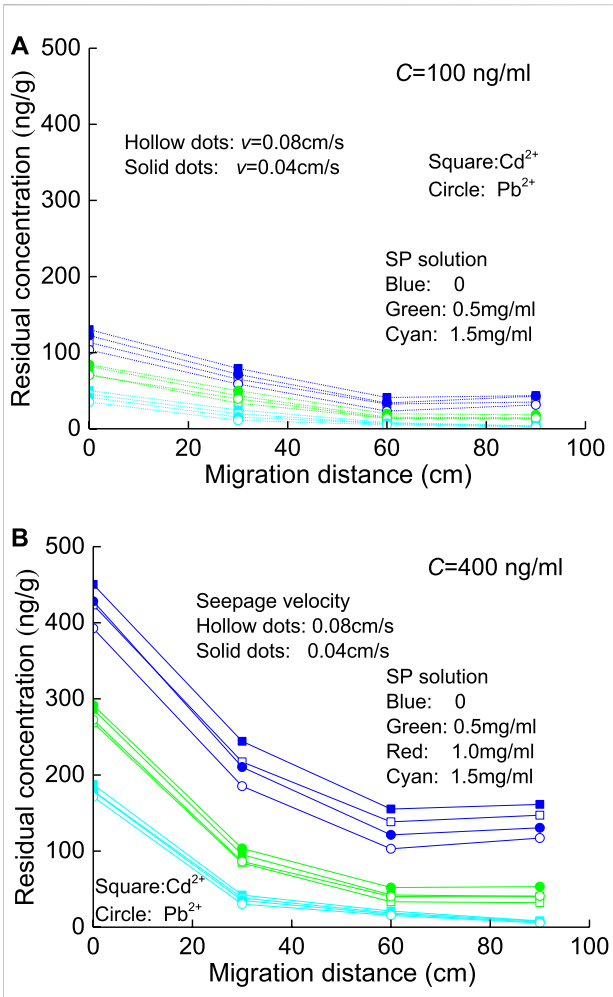

FIGURE 11
HM residues at each section of the sand column washed by SPs: **(A)** C=100 ng/ml and **(B)** C=400 ng/ml.

of the breakthrough curves and then tended to zero. For example, when the seepage velocity is v=0.08 cm/s, the concentration of Cd^{2+} solution is C=400 ng/ml, the injected SP concentration is C_{SP}=0.5 mg/ml, and the initial effluent concentration decreases to 282.59 ng/ml (hollow circles in Figure 9A) from 363.65 ng/ml (hollow squares in Figure 9A) and nearly decreases by 22.22%.

4.3 Migration distance under seepage flow

As shown in Figure 11, the increase in seepage velocity (e.g., v=0.04 cm/s→ 0.08 cm/s) reduces the residual content of HMs at different distances from the injection surface after cleaning. This phenomenon is more obvious when using deionized water (i.e., C_{SP}=0) for the flushing test due to the existence of a hydrodynamic effect. The high seepage velocity causes more HMs to attach to the desorbed quartz sand in the solution, which matches the phenomenon of the slightly higher effluent concentration mentioned above. With the addition of SP, the gap between the amounts of HMs desorbed from the quartz sand at the two seepage velocities (v=0.04 cm/s and 0.08 cm/s) is narrowing. On the other hand, some HMs that are not firmly bound to the quartz sand are adsorbed by the SP, while the HMs that are relatively firmly bound to the quartz sand enter the cleaning solution; this adsorption will increase with the increase in SP.

The previous discussion showed that the adsorption of Cd^{2+} and Pb^{2+} on SP is very different in the static adsorption process, but there is no significant difference in the effluent concentration in the seepage adsorption test. The reason is that the contact time between SP and HMs in the flow process is relatively short, and there is only surface adsorption. However, at each section of the sand column, the SP has sufficient contact time with HMs, and further adsorption reactions can occur, resulting in possible differences in the adsorption of Cd^{2+} and Pb^{2+} on SP (Figure 11). After the washing test with SPs, the residual concentration of Pb^{2+} at each section of the sand column is slightly lower than that of Cd^{2+} (e.g., Figure 11A; blue curves). This phenomenon showed that the adsorption reaction between SP and Pb^{2+} on the quartz sand at the cross sections is stronger than that of Cd^{2+}. Moreover, as the concentration of SP increases (e.g., C=100 ng/ml→400 ng/ml; Figure 11A), the difference between the residual concentrations of HMs dramatically increases.

According to these characteristics of the migration of SP in the sand column, it is of certain significance to control the migration of pollutants by controlling the seepage velocity, the SP concentration and the soil layer thickness in practical applications.

5 Conclusion

The adsorption of HMs (e.g., Cd^{2+} and Pb^{2+}) on SP can be divided into three stages: the surface adsorption stage, which mainly depends on the fastest adsorption due to physical processes; the internal pore diffusion stage, in which physical adsorption and chemical adsorption are combined; and the equilibrium stage, in which the adsorption amount does not change significantly, and the adsorption is in dynamic equilibrium.

The dissolution amount of HM-contaminated soil is very limited in a neutral environment, and at this time, the addition of SP has little effect. In the acid leaching test, after replacing the laterite with a certain amount of SP, the leaching amount of HMs decreased, which showed that SPs showed stronger adsorption for Cd^{2+} and Pb^{2+} in the competitive adsorption between SPs and laterite. In Pb^{2+}-contaminated soil, as long as the standing time is sufficient, the leaching concentration of HMs can reach the national standard regardless of whether the SP is added. In an acidic environment, there are more free HMs, so the harm to the surrounding environment of the soil is higher, and the SP has a greater impact on the concentration of HMs in the leaching

solution. Therefore, SPs can play a role in the treatment of heavy metal pollution in soil.

There are certain differences between Cd^{2+} and Pb^{2+} in the process of dynamic adsorption. The concentration of Pb^{2+} in the effluent is slightly lower than that of Cd^{2+}, and the residual concentration of Pb^{2+} at the cross-section is higher than that of Cd^{2+}. The residual concentration of Pb^{2+} at the cross-section after washing with SP solution is lower than that of Cd^{2+}. SPs have a better effect on the treatment of Pb^{2+}-contaminated soil than on Cd^{2+}-contaminated soil. Overall, SPs possess high purification efficiency for the HMs of contaminated soils.

Data availability statement

The original contributions presented in the study are included in the article/supplementary material, further inquiries can be directed to the corresponding author.

Author contributions

The main contribution of BB in this paper is methodology, and the other authors (BF, SC, NQ and SS) contributed in investigation and analysis.

Funding

This research was funded by the Beijing Natural Science Foundation (82222023) and National Natural Science Foundation of China (52079003).

Conflict of interest

Author QN was employed by China Hebei Construction and Geotechnical Investigation Group Ltd.

The remaining authors declare that the research was conducted in the absence of any commercial or financial relationships that could be construed as a potential conflict of interest.

Publisher's note

All claims expressed in this article are solely those of the authors and do not necessarily represent those of their affiliated organizations, or those of the publisher, the editors, and the reviewers. Any product that may be evaluated in this article, or claim that may be made by its manufacturer, is not guaranteed or endorsed by the publisher.

References

Abdelhafez, A. A., Li, J., and Abbas, M. H. H. (2014). Feasibility of biochar manufactured from organic wastes on the stabilization of heavy metals in a metal smelter contaminated soil. *Chemosphere* 117, 66–71. doi:10.1016/j.chemosphere.2014.05.086

Ahmad, M., Moon, D. H., Wazne, M., Kim, H. J., Lee, Y. H., and Ok, Y. S. (2013). Effects of natural and calcined oyster shells on antimony solubility in shooting range soil. *J. Korean Soc. Appl. Biol. Chem.* 56 (4), 461–464. doi:10.1007/s13765-012-3188-9

Bai, B., Fan, B., Li, X., Nie, Q., Jia, X., and Wu, H. (2022a). The remediation efficiency of heavy metal pollutants in water by industrial red mud particle waste. *Environ. Technol. Innovation* 28, 102944. doi:10.1016/j.eti.2022.102944

Bai, B., Jiang, S., Liu, L., Li, X., and Wu, H. (2021b). The transport of silica powders and lead ions under unsteady flow and variable injection concentrations. *Powder Technol.* 387, 22–30. doi:10.1016/j.powtec.2021.04.014

Bai, B., Nie, Q., Zhang, Y., Wang, X., and Hu, W. (2021a). Cotransport of heavy metals and SiO2 particles at different temperatures by seepage. *J. Hydrology* 597, 125771. doi:10.1016/j.jhydrol.2020.125771

Bai, B., Wang, Y., Rao, D., and Fan, B. (2022b). The effective thermal conductivity of unsaturated porous media deduced by pore-scale SPH simulation. *Front. Earth Sci. (Lausanne).* 10. doi:10.3389/feart.2022.943853

Bai, X., Cheng, W., and Li, G. (2021). A comparative study of different machine learning algorithms in predicting EPB shield behaviour: A case study at the xi'an metro, China. *Acta Geotech.* 16 (12), 4061–4080. doi:10.1007/s11440-021-01383-7

Bashir, S., Shaaban, M., Hussain, Q., Mehmood, S., Zhu, J., Fu, Q., et al. (2018). Influence of organic and inorganic passivators on Cd and Pb stabilization and microbial biomass in a contaminated paddy soil. *J. Soils Sediments* 18 (9), 2948–2959. doi:10.1007/s11368-018-1981-8

Chang, Z., Du, Z., Zhang, F., Huang, F., Chen, J., Li, W., et al. (2020). Landslide susceptibility prediction based on remote sensing images and GIS: Comparisons of supervised and unsupervised machine learning models. *Remote Sens.* 12, 502. doi:10.3390/rs12030502

Cui, X., Fan, Y., Wang, H., and Huang, S. (2019). Experimental investigation of suspended particles transport in porous medium under variable temperatures. *Hydrol. Process.* 33 (7), 1117–1126. doi:10.1002/hyp.13390

Cui, X., Li, J., Fei, W., Wen, T., Ding, S., He, S., et al. (2022a). Migration and deposition behavior of silica powder in saturated sand: Coupled effects of temperature and flow rate. *Granul. Matter* 24, 95. doi:10.1007/s10035-022-01254-2

Cui, X., Wu, D., Wang, H., Ding, S., and Fan, Y. (2022b). Pore features and seepage characteristics of natural gap graded sand with two size distributions. *Géotechnique* 72, 1–12. doi:10.1680/jgeot.21.00213

de Oliveira, L. H., Trigueiro, P., Rigaud, B., da Silva, E. C., Osajima, J. A., Fonseca, M. G., et al. (2021). When RNA meets montmorillonite: Influence of the pH and divalent cations. *Appl. Clay Sci.* 214, 106234. doi:10.1016/j.clay.2021.106234

Dehghan, P., Abbasi, M., Mofarahi, M., and Azari, A. (2021). Adsorption of synthetic and real kinetic hydrate inhibitors (KHI) wastewaters on activated carbon: Adsorption kinetics, isotherms, and optimized conditions. *Sep. Sci. Technol.* 56 (13), 2266–2277. doi:10.1080/01496395.2020.1821220

Deng, Y., Lu, X., Li, L., Xu, S., Miao, C., and Zhang, B. (2022). Experimental study on dynamic response of micron aluminum powder. *Granul. Matter* 24, 81. doi:10.1007/s10035-022-01248-0

Fan, B., Wu, W., Fu, L., Zhou, Q., Zhang, H., and Liu, Q. (2021). Preparation of magnetic shell powder for adsorption of nitrogen and phosphorus pollution in water. *Fresenius Environ. Bull.* 30 (6B), 7647–7653.

Hong, C. O., Kim, S. Y., Gutierrez, J., Owens, V. N., and Kim, P. J. (2010). Comparison of oyster shell and calcium hydroxide as liming materials for immobilizing cadmium in upland soil. *Biol. Fertil. Soils* 46 (5), 491–498. doi:10.1007/s00374-010-0458-8

Hu, W., Cheng, W., Wen, S., and Rahman, M. (2021a). Effects of chemical contamination on microscale structural characteristics of intact loess and resultant macroscale mechanical properties. *Catena* 203, 105361. doi:10.1016/j.catena.2021.105361

Hu, W., Cheng, W., Wen, S., and Yuan, K. (2021b). Revealing the enhancement and degradation mechanisms affecting the performance of carbonate precipitation in EICP process. *Front. Bioeng. Biotechnol.* 9, 750258. doi:10.3389/fbioe.2021.750258

Huang, F., Cao, Z., Guo, J., Jiang, S-H., Guo, Z., and Guo, Z. (2020a). Comparisons of heuristic, general statistical and machine learning models for landslide susceptibility prediction and mapping. *CATENA* 191, 104580. doi:10.1016/j.catena.2020.104580

Huang, F., Cao, Z., Jiang, S-H., Zhou, C., Guo, Z., and Guo, Z. (2020c). Landslide susceptibility prediction based on a semi-supervised multiple-layer perceptron model. *Landslides* 17, 2919–2930. doi:10.1007/s10346-020-01473-9

Huang, F., Zhang, J., Zhou, C., Wang, Y., Huang, J., and Zhu, L. (2020b). A deep learning algorithm using a fully connected sparse autoencoder neural network for landslide susceptibility prediction. *Landslides* 17 (01), 217–229. doi:10.1007/s10346-019-01274-9

Jiang, S. H., Huang, J., Huang, F., Yang, J., Yao, C., and Zhou, C. (2018). Modelling of spatial variability of soil undrained shear strength by conditional random fields for slope reliability analysis. *Appl. Math. Model.* 63, 374–389. doi:10.1016/j.apm.2018.06.030

Khan, M. J., and Jones, D. L. (2009). Effect of composts, lime and diammonium phosphate on the phytoavailability of heavy metals in a copper mine tailing soil. *Pedosphere* 19 (5), 631–641. doi:10.1016/s1002-0160(09)60158-2

Khirul, M. A., Kim, B. G., Cho, D., and Kwon, S. H. (2020). The effect of recycled waste oyster shell powder applied to organically enriched marine sediment as oxygen releasing compound. *Indian J. Geo-Marine Sci.* 49 (11), 1701–1709.

Lee, H. H., Kim, S. Y., Owens, V. N., Park, S., Kim, J., and Hong, C. O. (2018). How does oyster shell immobilize cadmium? *Arch. Environ. Contam. Toxicol.* 74 (1), 114–120. doi:10.1007/s00244-017-0453-2

Li, F., Huang, Y., Zhang, Y., Wang, M., Chen, L., and Jia, Y. (2021). Flotation and adsorption mechanism studies of antimony sulfide with 5-heptyl-1, 3, 4-oxadiazole-2-thione as a collector. *Miner. Eng.* 172, 107164. doi:10.1016/j.mineng.2021.107164

Li, H., Liu, Y., Zhou, Y., Zhang, J., Mao, Q., Yang, Y., et al. (2018). Effects of red mud based passivator on the transformation of Cd fraction in acidic Cd-polluted paddy soil and Cd absorption in rice. *Sci. Total Environ.* 640, 736–745. doi:10.1016/j.scitotenv.2018.05.327

Li, L., Zeng, Z., Wang, Z., Peng, Z., She, X., Li, S., et al. (2017). Effect of oyster shell powder loading on the mechanical and thermal properties of natural rubber/oyster shell composites. *Polym. Polym. Compos.* 25 (1), 17–22. doi:10.1177/096739111702500103

Liu, X. (2015). *Implement soil protection and build soil safety*. China Mining News, 6.

Mehmood, S., Imtiaz, M., Bashir, S., Rizwan, M., Irshad, S., Yuvaraja, G., et al. (2019). Leaching behavior of Pb and Cd and transformation of their speciation in co-contaminated soil receiving different passivators. *Environ. Eng. Sci.* 36 (6), 749–759. doi:10.1089/ees.2018.0503

Meski, S., Tazibt, N., Khireddine, H., Ziani, S., Biba, W., Yala, S., et al. (2019). Synthesis of hydroxyapatite from mussel shells for effective adsorption of aqueous Cd(II). *Water Sci. Technol.* 80 (7), 1226–1237. doi:10.2166/wst.2019.366

Moon, D. H., Cheong, K. H., Khim, J., Wazne, M., Hyun, S., Park, J. H., et al. (2013a). Stabilization of Pb2+ and Cu2+ contaminated firing range soil using calcined oyster shells and waste cow bones. *Chemosphere* 91 (9), 1349–1354. doi:10.1016/j.chemosphere.2013.02.007

Moon, D. H., Park, J. W., Cheong, K. H., Hyun, S., Koutsospyros, A., Park, J. H., et al. (2013b). Stabilization of lead and copper contaminated firing range soil using calcined oyster shells and fly ash. *Environ. Geochem. Health* 35 (6), 705–714. doi:10.1007/s10653-013-9528-9

Rodriguez-Arellao, G., Barajas-Fernandz, J., Garcia-Alamilla, R., Lagunes-Galvez, L. M., Lara-Rivera, A. H., and Garcia-Alamilla, P. (2021). Evaluation of cocoa beans shell powder as a bioadsorbent of Congo red dye aqueous solutions. *Materials* 14 (11), 2763. doi:10.3390/ma14112763

Sarkaya, A. G. (2021). Kinetic and thermodynamic studies of the biosorption of Cr (VI) in aqueous solutions by Agaricus campestris. *Environ. Technol.* 42 (1), 72–80. doi:10.1080/09593330.2019.1620867

State Environmental Protection Administration (2007a). *Solid waste-extraction procedure for leaching toxicity-sulphuric acid and nitric acid method: HJ/T299-2007*. China Environmental Science Press.

State Environmental Protection Administration (2007b). *State administration of quality supervision, inspection and quarantine. Identification standards for hazardous wastes-identification for extraction toxicity: GB 5085.3-2007*. China Environmental Science Press.

Torres-Quiroz, C., Dissanayake, J., and Park, J. (2021). Oyster shell powder, zeolite and red mud as binders for immobilising toxic metals in fine granular contaminated soils (from industrial zones in South Korea). *Int. J. Environ. Res. Public Health* 18 (5), 2530. doi:10.3390/ijerph18052530

Wang, H., Xing, H., Yan, K., Han, D., and Chen, J. (2022). Oyster shell derived hydroxyapatite microspheres as an effective adsorbent for remediation of Coomassie brilliant blue. *Adv. Powder Technol.* 33 (2), 103425. doi:10.1016/j.apt.2022.103425

Wang, Q., Jiang, F., Ouyang, X., Yang, L., and Wang, Y. (2021). Adsorption of Pb(II) from aqueous solution by mussel shell-based adsorbent: Preparation, characterization, and adsorption performance. *Materials* 14 (4), 741. doi:10.3390/ma14040741

Wu, K., Huang, W., Hung, W., and Tsai, C. W. (2021). Modified expanded graphite/Fe3O4 composite as an adsorbent of methylene blue: Adsorption kinetics and isotherms. *Mater. Sci. Eng. B* 266, 115068. doi:10.1016/j.mseb.2021.115068

Xu, X., Liu, X., Oh, M., and Park, J. (2019). Oyster shell as a low-cost adsorbent for removing heavy metal ions from wastewater. *Pol. J. Environ. Stud.* 28 (4), 2949–2959. doi:10.15244/pjoes/92941

Xue, Z., Cheng, W., Wang, L., and Hu, W. (2022). Effects of bacterial inoculation and calcium source on microbial-induced carbonate precipitation for lead remediation. *J. Hazard. Mater.* 426, 128090. doi:10.1016/j.jhazmat.2021.128090

Yakub, E., Agarry, S., Omoruwou, F., and Owabor, C. N. (2020). Comparative study of the batch adsorption kinetics and mass transfer in phenol-sand and phenol-clay adsorption systems. *Part. Sci. Technol.* 38 (7), 801–811. doi:10.1080/02726351.2019.1616862

Yu, T., Jiang, T., Liu, X., Ma, X., and Yang, Z. (2021). Current situation of soil heavy metal pollution and research progress of detection and analysis technology. *Geol. China* 48 (2), 460–476.

Zhai, Q., Lu, H., Liu, R., He, D., Wang, C., and Sun, W. (2021). Removal of suspended solids from weathered tungsten-ore beneficiation wastewater by electroneutralization and chemical precipitation. *Miner. Eng.* 173, 107167. doi:10.1016/j.mineng.2021.107167

Zhang, W., Long, A., Ou, J., Zeng, X., Wang, J., Wang, B., et al. (2021). Enhanced removal of hexavalent chromium from aqueous solution by functional polymer-wrapped gamma-alumina composite adsorbent. *Environ. Technol. Innovation* 24, 101954. doi:10.1016/j.eti.2021.101954

Zhong, G., Liu, Y., and Tang, Y. (2021). Oyster shell powder for Pb(II) immobilization in both aquatic and sediment environments. *Environ. Geochem. Health* 43 (5), 1891–1902. doi:10.1007/s10653-020-00768-z

Zhou, F., Huang, S., Liu, X., Feng, J., Liu, Q., Zhiwei, W., et al. (2021). Adsorption kinetics and thermodynamics of rare Earth on Montmorillonite modified by sulfuric acid. *Colloids Surfaces A Physicochem. Eng. Aspects* 627, 127063. doi:10.1016/j.colsurfa.2021.127063